# Asymmetric Boronate Addition to *o*-Quinone Methides: Ligand Exchange, Solvent Effects, and Lewis Acid Catalysis

Matthew N. Grayson and Jonathan M. Goodman*

Centre for Molecular Science Informatics, Department of Chemistry, University of Cambridge, Lensfield Road, Cambridge CB2 1EW, United Kingdom

Ⓢ *Supporting Information*

ABSTRACT: Density functional theory calculations suggest that asymmetric boronate addition to *o*-quinone methides proceeds via a Lewis acid catalyzed process through a closed six-membered transition structure. The BINOL-derived catalyst undergoes an exchange process with the original ethoxide boronate ligands. This activation mode successfully accounts for the sense and level of enantioselectivity observed experimentally. A qualitative model which accurately predicts the observed enantioselectivity has been developed and is consistent with results from our study of ketone propargylation demonstrating the reaction model's generality. The effects of replacing the BINOL framework with H_8−BINOL have been rationalized.
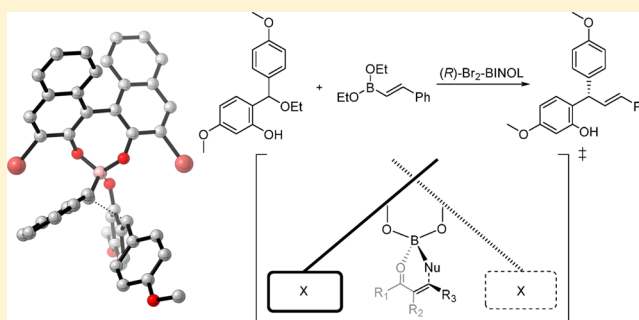
1. INTRODUCTION

o-Quinone methides (*o*QMs) have been proposed as key reactive intermediates in the total synthesis of many natural products including carpanone,[1] tectol,[2] and rubioncolin A.[3] Notable reactions involving *o*QMs include hetero-Diels−Alder reactions[4,5] and nucleophilic addition at the exocyclic carbon in 1,4-conjugate addition reactions.[6]

The catalytic asymmetric conjugate addition of nucleophiles to *o*QMs has recently attracted much synthetic attention.[7,8] In 2012, Luan and Schaus reported using a BINOL-derived chiral diol as an effective promoter of boronate addition to *o*QMs (Scheme 1).[9] This reaction class has synthetic applications for bioactive natural products such as (+)-myristinin A,[10] (*S*)- and (*R*)-tolterodine,[11] and (−)-(*S*)-4-methoxydalbergione.[12] However, it is unclear how the chiral diol catalyzes the reaction. A full understanding of selectivity-controlling factors enables rational design of further experimental work, helping develop this and related transformations. Moreover, exploration of this reaction would give us an insight into the generality of the reaction model we have developed for ketone propargylation.[13]

Previous work examining similar chiral diol-catalyzed reactions showed binaphthol-associated boronates to be responsible for the observed catalytic effects.[14] Schaus had previously proposed a Brønsted acid catalyzed pathway in which the original ligand and diol are both covalently attached to a boron atom to explain the outcome of related reactions.[15,16] However, it has been found that to explain the experimental observations, a Lewis acidic species derived from the complete displacement of the original ligand(s) is required.[17]

Herein, we report the results of DFT calculations that provide a mechanistic insight into this important transformation.

The results of these calculations indicate that the reaction proceeds via a six-membered ring sofa-like transition structure (TS) corresponding to a Lewis acid type activation mode in which the chiral diol completely displaces the original boronate ligands. This pathway accurately reproduces the experimentally observed enantioselectivity. A qualitative model has also been developed which accurately predicts the observed enantioselectivity and agrees with results from our study of ketone propargylation demonstrating the generality of this reaction model.

2. COMPUTATIONAL DETAILS

The B3LYP density functional[18,19] and split-valence polarized 6-31G** basis set[20,21] were used for all geometry optimizations. All activation free energies are quoted relative to infinitely separated reagents. Quantum mechanical calculations were performed using Gaussian03 (Revision E.01).[22] Single-point energies were taken using the M06-2X density functional[23] and LACVP** basis set[24] using the Jaguar program (version 7.6).[25] This energy was used to correct the gas-phase energy obtained from the B3LYP calculations.[26−28]

Free energies in solution were derived from gas-phase-optimized structures (B3LYP/6-31G**) by means of a single-point calculation using M06-2X/LACVP** with the polarizable continuum model (PCM),[29] as implemented in the Jaguar program (version 7.6). These values were used to correct the Gibbs free energy derived from the B3LYP calculations.
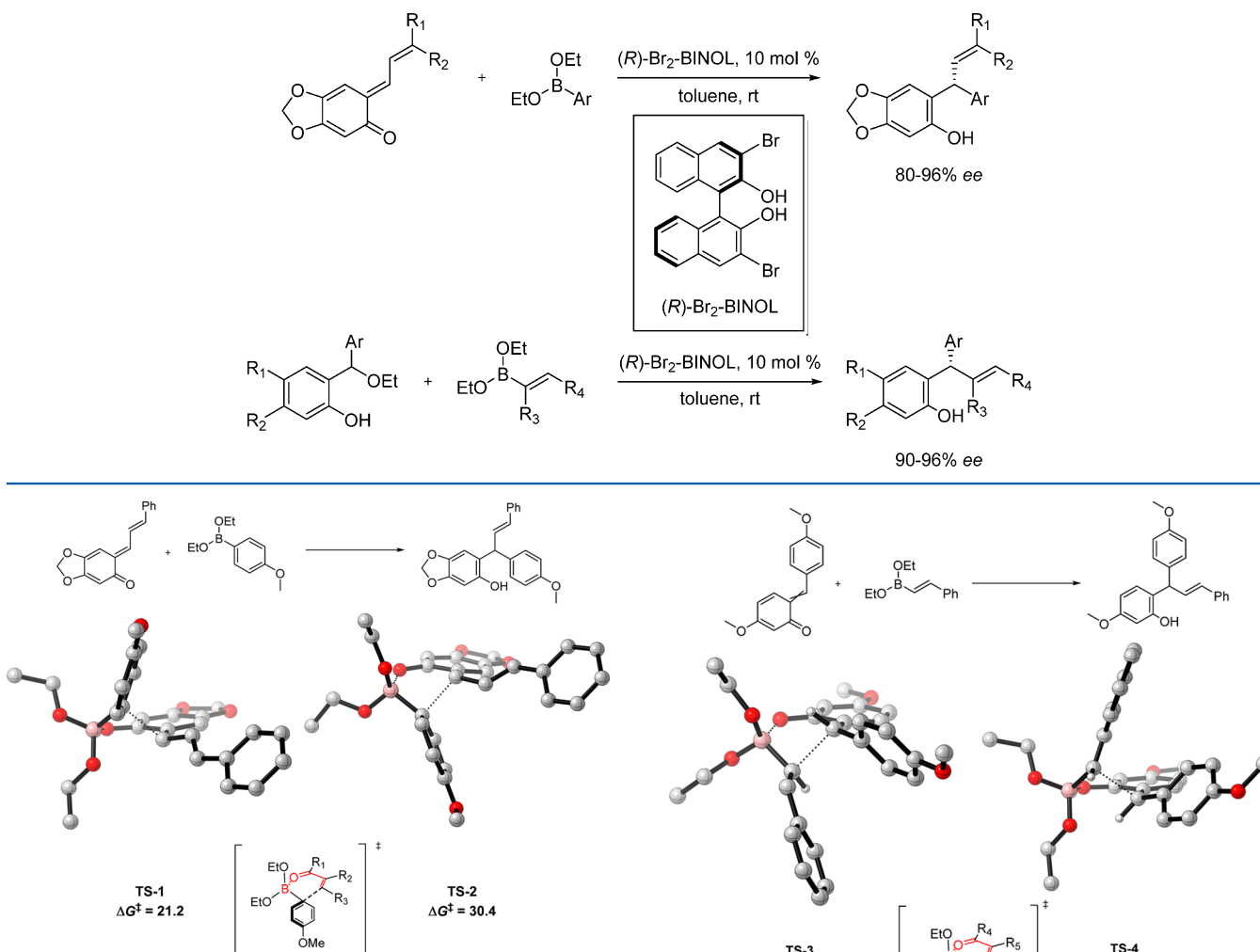
Scheme 1. Boronate Addition to *o*QMs[9]

Figure 1. Uncatalyzed TSs for arylboration. Geometries B3LYP/6-31G**, single-point energies M06-2X/6-31G**. All energies in kcal mol⁻¹.

3. RESULTS AND DISCUSSION

Investigation of uncatalyzed boronate addition to *o*QMs indicated that the reaction proceeds via a cyclic, six-membered ring sofa-like TS when both arylboronate and alkenylboronate nucleophiles were employed, **TS-1** and **TS-3**, respectively (Figures 1 and 2). The geometry of the side chain in the arylboration reaction was found to be important with the *cis* conformer (**TS-2**), calculated to be 9.2 kcal mol⁻¹ higher in energy than the *trans* (**TS-1**). A similar effect was observed for uncatalyzed alkenylboration with respect to the preferred nucleophile orientation. When the protons of the nucleophile and *o*QM at the reacting centers are *syn* (**TS-4**) the TS is destabilized by 2.9 kcal mol⁻¹ relative to **TS-3**, which benefits from the more sterically favorable *anti* arrangement.

The alkenylboration reaction relies upon the formation of the required *o*QM in situ which could lead to a mixture of double-bond geometries. The ground-state *Z* alkene was calculated to be disfavored by 1.9 kcal mol⁻¹ relative to the *E* alkene. Furthermore, the TSs corresponding to the *Z* alkene reaction, **TS-5** and **TS-6**, were found to be disfavored relative to **TS-3** (Figure 2).

In order to investigate the enantioselective effects observed in the catalyzed reaction, the energetics of ligand exchange between
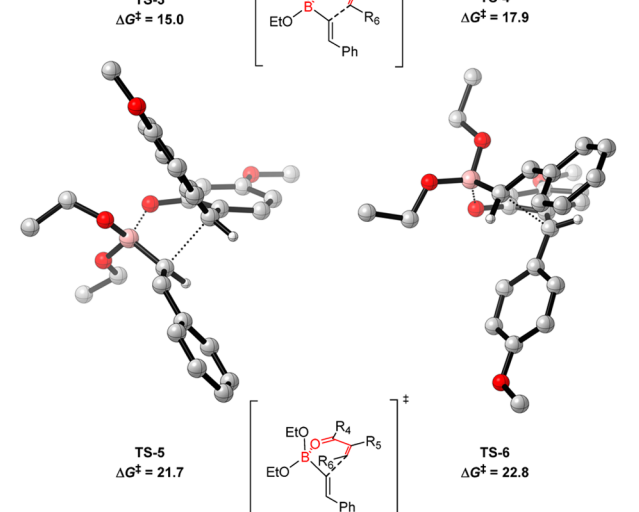

Figure 2. Uncatalyzed TSs for alkenylboration. Geometries B3LYP/6-31G**, single-point energies M06-2X/6-31G**. All energies in kcal mol⁻¹.

the chiral diol and boronate ligands were investigated. The thermodynamic stabilities of the chiral boronates were calculated, and **1a** and **1b** were found to be the predominant chiral boronates in their respective reaction mixtures, in agreement with previous work investigating similar reactions,[13,17,30] (Scheme 2). However, the Lewis acid catalysis promoted by **2a**

Scheme 2. Boronate Ligand-Exchange Energetics. Geometries B3LYP/6-31G**, Single-Point Energies M06-2X/LACVP**[a]
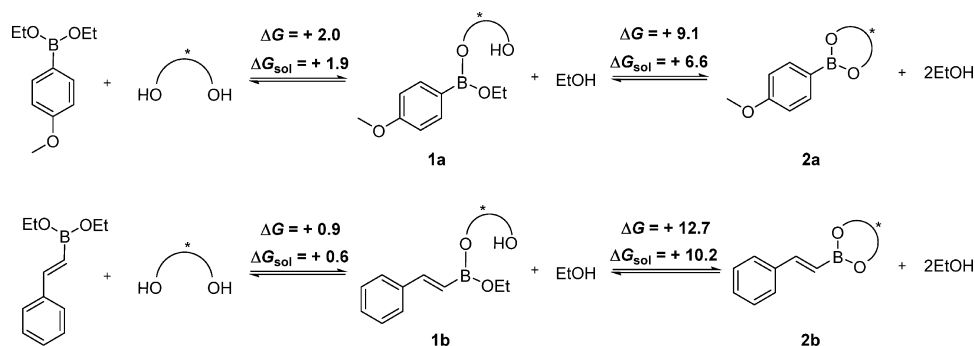
[a]All energies in kcal mol^{-1}.
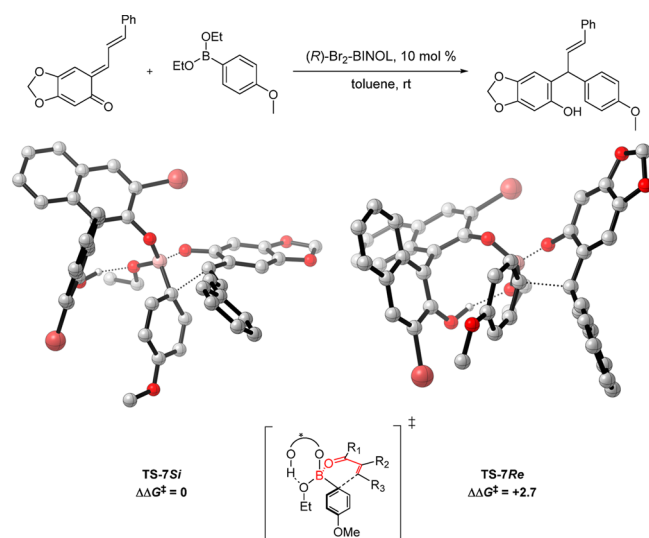
Figure 3. Competing TSs for the reaction of **1a**. Geometries B3LYP/6-31G**, single-point energies M06-2X/LACVP**. All energies in kcal mol^{-1}.
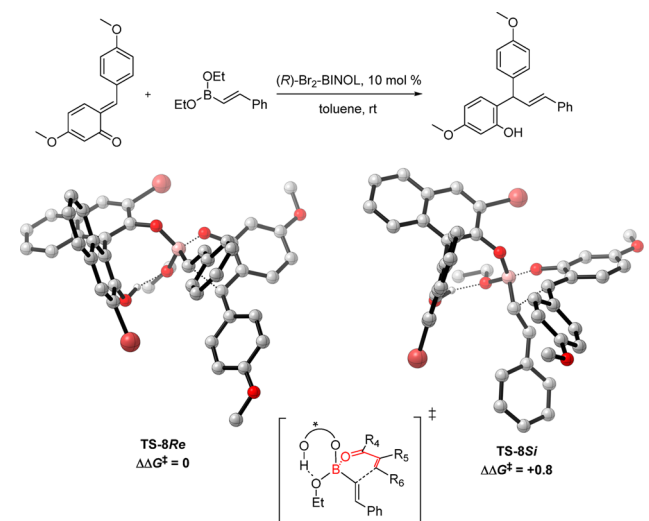
Figure 4. Competing TSs for the reaction of **1b**. Geometries B3LYP/6-31G**, single-point energies M06-2X/LACVP**. All energies in kcal mol^{-1}.

and **2b** may be more effective than the Brønsted acid catalysis of **1a** and **1b** even though they are present in lower concentrations. A similar ligand-exchange process has been reported by which

Table 1. Comparison of Arylboration Reaction Pathways[a]

	uncatalyzed	reaction with 1a	reaction with 2a
gas phase			
relative free energy of ligand exchange	0.0	2.0	11.1
$\Delta G^{\ddagger}$	21.2	13.0	5.5
overall barrier	21.2	*15.0*	16.6
solvent = toluene			
relative free energy of ligand exchange	0.0	1.9	8.5
$\Delta G^{\ddagger}$	23.8	17.0	7.5
overall barrier	23.8	18.9	*16.0*

[a]Free energies of ligand exchange relative to free catalyst and achiral boronate. Lowest energy pathway in italic. All energies in kcal mol^{-1}.

Table 2. Comparison of Alkenylboration Reaction Pathways[a]

	uncatalyzed	reaction with 1b	reaction with 2b
gas phase			
relative free energy of ligand exchange	0.0	0.9	13.6
$\Delta G^{\ddagger}$	15.0	8.9	−5.1
overall barrier	15.0	9.8	8.5
solvent = toluene			
relative free energy of ligand exchange	0.0	0.6	10.8
$\Delta G^{\ddagger}$	17.4	11.9	−2.6
overall barrier	17.4	12.5	8.2

[a]Free energies of ligand exchange relative to free catalyst and achiral boronate. Lowest energy pathway in italic. All energies in kcal mol^{-1}.

the higher energy Lewis acid catalyzes the major pathway for a reaction,[14] and so these thermodynamic calculations in isolation do not allow the preferred mechanisms to be determined.

Armstrong and co-workers state that a triple-ζ quality basis set, such as tzvp, is required to remove significant basis set superposition errors (BSSE) when comparing competing organic reactions.[31] Therefore, the structures in Scheme 2 corresponding to arylboration were reoptimized at the B3LYP/tzvp level of theory in Gaussian. Single-point energies were taken using the M06-2X density functional in Jaguar to correct the energies obtained from the B3LYP calculations. The average changes in relative free energies of ligand exchange at this new level of theory compared to the 6-31G** derived values were 1.2 kcal mol^{-1} in the gas phase and 1.3 kcal mol^{-1} in the solvent phase, which

Figure 5. Competing TSs for the reaction of **2a**. Geometries B3LYP/6-31G**, single-point energies M06-2X/LACVP**. All energies in kcal mol⁻¹.
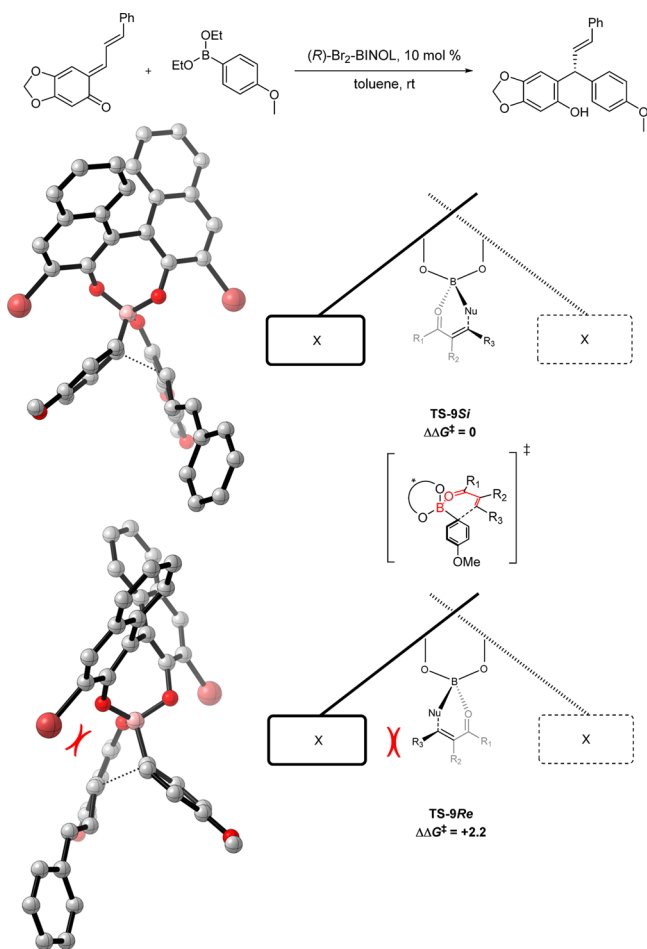

Figure 6. Competing TSs for the reaction of **2b**. Geometries B3LYP/6-31G**, single-point energies M06-2X/LACVP**. All energies in kcal mol⁻¹.

resulted in the same trend in ligand energetics as calculated using 6-31G**. This suggests that the effects of BSSE can be assumed to be of a magnitude small enough to be ignore and is a result of the similar connectivity and the presence of mainly light elements in these organic molecules.

The activation free energy for the reaction of **1a** and **1b** with *o*QMs was found to be 13.0 and 8.9 kcal mol⁻¹, respectively, when evaluated using M06-2X/LACVP**, and both reaction barriers are lower than their respective uncatalyzed reactions. This can be attributed to a Brønsted acid type activation mode in which the remaining catalyst hydroxyl group forms a hydrogen-bonding interaction to the remaining ethoxide ligand (Figures 3 and 4). This activated boron center leads to a stronger association of the *o*QM and a tighter TS than the corresponding uncatalyzed process. 22 and 31 unique TSs were located for arylboration and alkenylboration, respectively, due to the flexibility of this activation mode. **TS-7Re** and **TS-7Si** (Figure 3) and **TS-8Re** and **TS-8Si** (Figure 4) were the lowest energy TSs located. *R* and *S* chirality on boron were considered for both aryl- and alkenylboration reactions. The *R* configuration was found to be higher in energy in both reactions relative to *S*, which is in agreement with work that examined a similar reaction.[14]

The activation free energies for the reaction of **2a** and **2b** and their corresponding electrophiles were calculated as lower than the barriers for both the uncatalyzed and Brønsted acid catalyzed pathways (Tables 1 and 2). Compounds **2a** and **2b** are
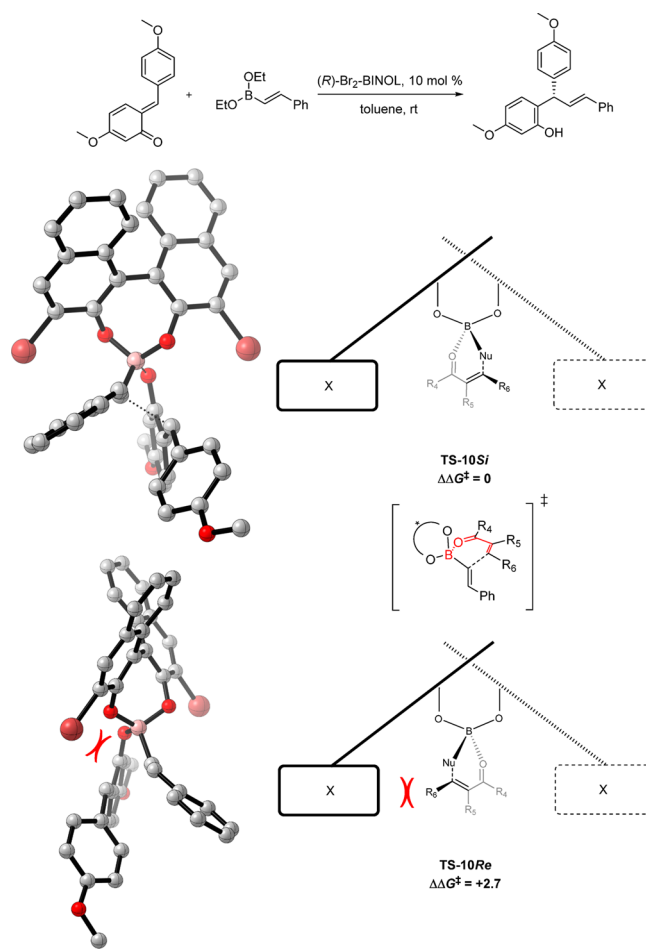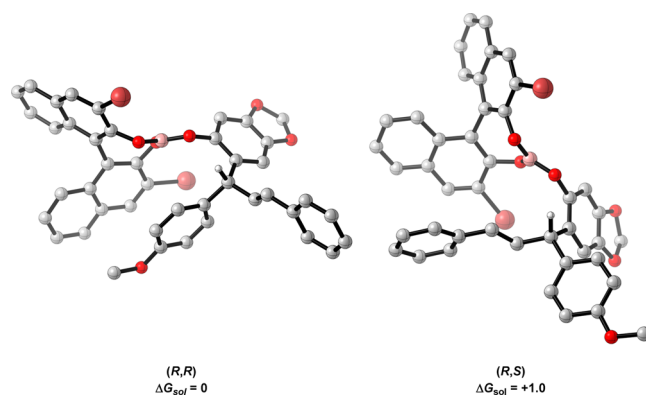

Figure 7. Thermodynamic stability of the diastereomeric arylboration product complexes. All energies in kcal mol⁻¹.

nonplanar, which prevents delocalization of the oxygen lone pairs into the empty boron p orbital, making them effective Lewis acids. **TS-9Si** and **TS-10Si** were found to be favored relative to **TS-9Re** and **TS-10Re** (Figures 5 and 6). Using the calculated Boltzmann ratios at 298 K, the predicted er is 97.5:2.5 and 99:1 for arylboration and alkenylboration respectively, in close agreement with the experimentally observed enantioselectivity (97:3 and 97.5:2.5 er).

By assuming that the original and chiral boronates are in equilibrium, Curtin−Hammett conditions apply, and therefore,
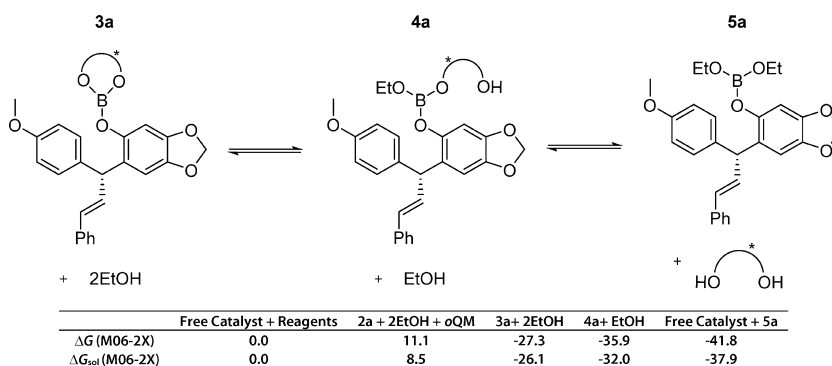
	Free Catalyst + Reagents	2a + 2EtOH + oQM	3a+ 2EtOH	4a+ EtOH	Free Catalyst + 5a
ΔG (M06-2X)	0.0	11.1	-27.3	-35.9	-41.8
ΔG_{sol} (M06-2X)	0.0	8.5	-26.1	-32.0	-37.9

Figure 8. Boronate product ligand-exchange equilibria and thermodynamics of catalyst turnover. All energies in kcal mol^{-1}.
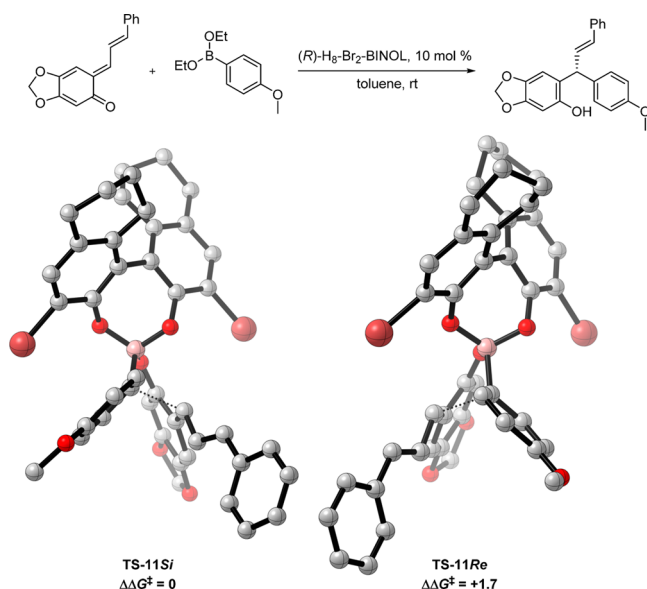

Figure 9. Competing TSs for arylboration with (R)-H$_8$−Br$_2$-BINOL as the catalyst. Geometries B3LYP/6-31G**, single-point energies M06-2X/LACVP**. All energies in kcal mol^{-1}.

the favored pathway is determined by the absolute energies of the TSs.[32] In the gas phase, these conditions indicate that the preferred pathways are via reaction of **1a** and **2b** for arylboration and alkenylboration, respectively (Tables 1 and 2).

Under Curtin−Hammett conditions, solvation shows that reaction of **2a** and **2b** are the preferred pathways (Tables 1 and 2). This reversal in arylboration pathway preference and strengthening of alkenylboration pathway preference is due to the more polarized intermediates and TSs relative to the starting materials and highlights the need to rigorously assess solvent effects when computationally investigating competing organic reactions.[33]

Solvation of **TS-9Re** and **TS-9Si** led to an increase in relative free energy of just 0.3 kcal mol^{-1}. Solvation of **TS-10Re** and **TS-10Si** led to a decrease in relative free energy of just 0.5 kcal mol^{-1}. These minor changes upon solvation show that gas phase calculations are a reasonable approximation for competing TSs within the same reaction mechanism and can be attributed to similar levels of charge development in the TSs.[28]

The observed selectivity can be rationalized by considering a projection of the catalyst down the central carbon−carbon single bond (Figures 5 and 6). The oQM side chain clashes with the catalyst bromine atom in the case of **TS-9Re** and **TS-10Re**. In **TS-9Si** and **TS-10Si**, this side chain is placed in the catalyst empty pocket at the front of this projection, stabilizing these TSs relative to **TS-9Re** and **TS-10Re** and leading to the experimentally observed selectivity. These results are consistent with the findings from the study of ketone propargylation demonstrating the generality of this reaction model.[13]

Under the experimental reaction conditions, the C−C bond-forming step could be reversible. To investigate this, the two diastereomeric product complexes which are formed after C−C bond formation in arylboration, which should also be representative of alkenylboration, were located. They were calculated to be within 1.0 kcal mol^{-1} of each other in solution (Figure 7). Examination of the full catalytic cycle indicated that arylboration via reaction of **2a** and subsequent chiral catalyst release has a $\Delta_r G_{sol}$ value of −37.9 kcal mol^{-1} (Figure 8). The large thermodynamic driving force for this reaction is due to the generation of aromaticity in the product. The product, therefore, acts as a thermodynamic sink for the reagents, and consequently, under the standard conditions, the reaction proceeds under kinetic control via **TS-9Si**.

To test this mechanistic understanding, the arylboration reaction in which the (R)-Br$_2$-BINOL catalyst was replaced by (R)-H$_8$−Br$_2$-BINOL was examined (Figure 9). Hydrogenation of the rear aromatic rings reduces the enantioselective effect of the catalyst, and the observed experimental enantiomeric ratio was reported to be 74:26.[9] **TS-11Re** and **TS-11Si** show that this trend is correct with the energy difference between the TSs calculated to be 1.7 kcal mol^{-1}, falling from 2.2 kcal mol^{-1} in the case of **TS-9Re** and **TS-9Si**. This effect can be rationalized by considering the qualitative model presented in Figure 5. The sp^3 centers of the two rear rings are more sterically demanding than the sp^2 centers of the two aromatic rings prior to hydrogenation. This larger steric clash increases the dihedral angle defined by both naphthyl groups (described by carbons 2, 1, 1′, and 2′, where 2 and 2′ are the oxygen-bearing carbons) from 52 to 56°. The effect of this is to move the bromine atoms away from the catalyst active site, reducing their interaction with the substrate, lowering enantioselectivity. To the best of our knowledge, this constitutes the first mechanistic work toward understanding the difference between these two chiral frameworks.

The arylboration reaction in which the (R)-Br$_2$-BINOL catalyst was replaced by (R,R)-tartaric acid was also examined (**TS-12Re** and **TS-12Si**, Figure 10). Experimentally, this catalyst was reported to yield an enantiomeric ratio of 52:48, the lowest enantioselectivity of all diol catalysts tested.[9] The energy difference between the TSs was calculated to be just 0.8 kcal mol^{-1}, in agreement with the experimental results. Using the qualitative model developed, the loss of selectivity can be
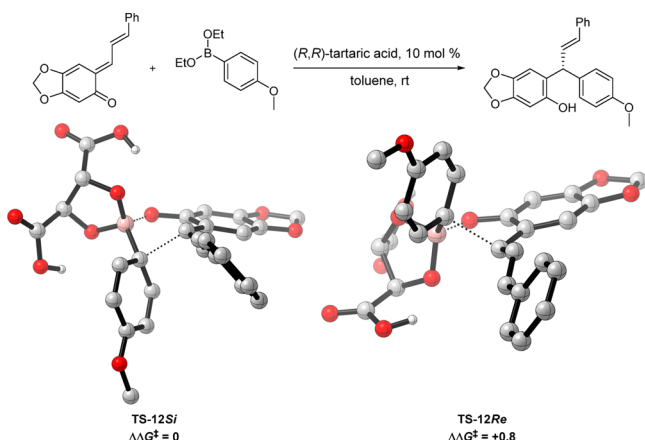
Figure 10. Competing TSs for arylboration with (*R,R*)-tartaric acid as the catalyst. Geometries B3LYP/6-31G**, single-point energies M06-2X/LACVP**. All energies in kcal mol^{-1}.

rationalized in terms of the lower steric demands of tartaric acid relative to the BINOL-derived scaffold.

4. CONCLUSION

DFT calculations suggest that asymmetric boronate addition to *o*-quinone methides proceeds via a Lewis acid catalyzed process through a closed six-membered TS. The BINOL-derived catalyst undergoes an exchange process with the original ethoxide boronate ligands. While displacement of one achiral ligand leads to the thermodynamically preferred chiral boronate, loss of both original boronate ligands results in the active catalyst species. This activation mode successfully accounts for the sense and level of enantioselectivity observed experimentally. A qualitative model accurately predicts the observed enantioselectivity and is consistent with results from our study of ketone propargylation, demonstrating the generality of this reaction model.

■ ASSOCIATED CONTENT

Ⓢ Supporting Information

Complete list of authors in the Gaussian03 reference; Cartesian coordinates, energies, and number of imaginary frequencies of all stationary points and values of imaginary frequencies of all transition structures. This material is available free of charge via the Internet at http://pubs.acs.org.

■ AUTHOR INFORMATION

Corresponding Author
*E-mail: jmg11@cam.ac.uk.
Notes
The authors declare no competing financial interest.

■ ACKNOWLEDGMENTS

■ REFERENCES

(1) Chapman, O. L.; Engel, M. R.; Springer, J. P.; Clardy, J. C. *J. Am. Chem. Soc.* **1971**, *93*, 6696−6698.
(2) Khanna, R. N.; Sharma, P. K.; Thomson, R. H. *J. Chem. Soc., Perkin Trans. 1* **1987**, 1821−1824.
(3) Lumb, J.-P.; Trauner, D. *J. Am. Chem. Soc.* **2005**, *127*, 2870−2871.
(4) Bray, C. D. *Org. Biomol. Chem.* **2008**, *6*, 2815−2819.
(5) Gharpure, S. J.; Sathiyanarayanan, A. M.; Vuram, P. K. *RSC Adv.* **2013**, *3*, 18279−18282.
(6) Selenski, C.; Pettus, T. R. R. *J. Org. Chem.* **2004**, *69*, 9196−9203.
(7) El-Sepelgy, O.; Haseloff, S.; Alamsetti, S. K.; Schneider, C. *Angew. Chem., Int. Ed.* **2014**, *53*, 7923−7927.
(8) Hsiao, C.-C.; Liao, H.-H.; Rueping, M. *Angew. Chem., Int. Ed.* **2014**, *53*, 13258−13263.
(9) Luan, Y.; Schaus, S. E. *J. Am. Chem. Soc.* **2012**, *134*, 19965−19968.
(10) Sawadjoon, S.; Kittakoop, P.; Kirtikara, K.; Vichai, V.; Tanticharoen, M.; Thebtaranonth, Y. *J. Org. Chem.* **2002**, *67*, 5470−5475.
(11) Ulgheri, F.; Marchetti, M.; Piccolo, O. *J. Org. Chem.* **2007**, *72*, 6056−6059.
(12) Bissel, P.; Nazih, A.; Sablong, R.; Lepoittevin, J.-P. *Org. Lett.* **1999**, *1*, 1283−1285.
(13) Grayson, M. N.; Goodman, J. M. *J. Org. Chem.* **2013**, *78*, 8796−8801.
(14) Paton, R. S.; Goodman, J. M.; Pellegrinet, S. C. *Org. Lett.* **2009**, *11*, 37−40.
(15) Lou, S.; Moquist, P. N.; Schaus, S. E. *J. Am. Chem. Soc.* **2006**, *128*, 12660−12661.
(16) Lou, S.; Moquist, P. N.; Schaus, S. E. *J. Am. Chem. Soc.* **2007**, *129*, 15398−15404.
(17) Paton, R. S.; Goodman, J. M.; Pellegrinet, S. C. *J. Org. Chem.* **2008**, *73*, 5078−5089.
(18) Becke, A. D. *Phys. Rev. A* **1988**, *38*, 3098−3100.
(19) Lee, C.; Yang, W.; Parr, R. G. *Phys. Rev. B* **1988**, *37*, 785−789.
(20) Krishnan, R.; Binkley, J. S.; Seeger, R.; Pople, J. A. *J. Chem. Phys.* **1980**, *72*, 650−654.
(21) Gill, P. M. W.; Johnson, B. G.; Pople, J. A.; Frisch, M. J. *Chem. Phys. Lett.* **1992**, *197*, 499−505.
(22) Frisch, M. J., et al. *Gaussian 03*; Gaussian, Inc., Wallingford, CT, 2004.
(23) Zhao, Y.; Truhlar, D. *Theor. Chem. Acc.* **2008**, *120*, 215−241.
(24) Hay, P. J.; Wadt, W. R. *J. Chem. Phys.* **1985**, *82*, 270−283.
(25) Jaguar, version 7.6, Schrodinger, LLC, New York, NY, 2009.
(26) Simón, L.; Goodman, J. M. *Org. Biomol. Chem.* **2011**, *9*, 689−700.
(27) Grayson, M. N.; Pellegrinet, S. C.; Goodman, J. M. *J. Am. Chem. Soc.* **2012**, *134*, 2716−2722.
(28) Grayson, M. N.; Goodman, J. M. *J. Am. Chem. Soc.* **2013**, *135*, 6142−6148.
(29) Mennucci, B.; Tomasi, J. *J. Chem. Phys.* **1997**, *106*, 5151−5158.
(30) Pellegrinet, S. C.; Goodman, J. M. *J. Am. Chem. Soc.* **2006**, *128*, 3116−3117.
(31) Armstrong, A.; Boto, R. A.; Dingwall, P.; Contreras-García, J.; Harvey, M. J.; Mason, N. J.; Rzepa, H. S. *Chem. Sci.* **2014**, *5*, 2057.
(32) Seeman, J. I. *Chem. Rev.* **1983**, *83*, 83−134.
(33) Dieckmann, A.; Breugst, M.; Houk, K. N. *J. Am. Chem. Soc.* **2013**, *135*, 3237−3242.